

NEOSSat observations of three transiting hot Jupiters

Chris Fox^{1,2}★ and Paul Wiegert^{1,2}

¹Department of Physics and Astronomy, The University of Western Ontario, London, Ontario N6A 3K7, Canada

²Institute for Earth and Space Exploration (IESX), The University of Western Ontario, London, Ontario N6A 3K7, Canada

Accepted 2022 September 3. Received 2022 September 1; in original form 2022 July 3

ABSTRACT

The *Near Earth Object Surveillance Satellite (NEOSSat)* is a Canadian-led 15 cm Earth-orbiting telescope originally designed to detect asteroids near the Sun. Its design is however also suitable for the observation of exoplanetary transits of bright stars. We used the *NEOSSat* platform to perform followup observations of several *Transiting Exoplanets Survey Satellite (TESS)* targets, both as a demonstration of *NEOSSat* capabilities for exoplanetary science and improve the orbital ephemerides and properties of these exoplanet systems. We are able to recover / confirm the orbital properties of such targets to within mutual error bars, demonstrating *NEOSSat* as a useful future contributor to exoplanetary science.

Key words: methods: numerical – techniques: photometric – telescopes – planets and satellites: detection – stars: individual: WASP-43 TOI-1516 TOI-2046.

1 INTRODUCTION

The *Near Earth Object Surveillance Satellite (NEOSSat)* (Laurin et al. 2008) is a Canadian microsatellite originally designed to detect and track near-Sun asteroids. About the size of a suitcase, *NEOSSat* orbits Earth in a Sun-synchronous orbit of approximately 100 min. It carries a 15 cm F/6 telescope with a limiting magnitude of $V = 19.5$ for a 100 s exposure. Its spectral range is 350 to 1050 nm, and has a field of view of 0.86×0.86 deg. These characteristics make it suitable for exoplanet transit studies of sufficiently bright stars.

Here we report on a campaign that used *NEOSSat* to perform followup observations of three exoplanets from the list of systems observed by the *Transiting Exoplanets Survey Satellite (TESS)* (Ricker et al. 2014). *TESS* has discovered thousands of new exoplanets, and many of these objects require followup observation to confirm or improve the transit ephemeris and other parameters.

Though we will use the *NEOSSat* data to determine specific parameters of our target systems, our motivation is primarily to assess the capabilities of *NEOSSat* itself: we aim to demonstrate that *NEOSSat* can be a useful platform for exoplanetary science; that it can produce reliable parameters that can be used in conjunction with other data sources to better characterize future exoplanetary candidates.

2 DATA PROCESSING

The data were obtained from *NEOSSat* on-orbit operations from 2021 March to 2022 June. Specific dates of our observations are reported when each system is discussed (below). Raw FITS images from each *NEOSSat* observing run were downloaded from their repository at the Canadian Astronomy Data Centre (CADC).

Exposure times for targets were as short as 5 s and as long as 20 s, with cadences of 10 s through 20 s. To avoid photometric saturation, we optimized the exposure times for each target so that the peak pixel count was one-third to one-half the maximum value (pixels are 16 bit, thus a maximum count of 65535). Observations of a single transit event typically included 300–600 individual observations; the exact number obtained depended on factors such as line-of-sight limitations, whether the satellite is over the South Atlantic Anomaly (SAA, where increased particle flux causes excessive noise in the raw images), and certain orbital and operational constraints (such as desaturation of the reaction wheels after the SAA and re-locking on to the target) result in observations typically being limited to less than one hour.

Once downloaded, we used differential photometry to extract the light curve of each target. This is a two-step process, based on cleaning and extraction code designed for the *NEOSSat* mission by Jason Rowe (Rowe 2020) and modified for our purposes. First, the cleaning algorithm removed instrumental effects (such as bias, electronic, and dark noise) and created a dark-subtracted set of science images. The second step is the extraction process. Stars are detected in the image using AstroPy's DAOPhot routine (Astropy Collaboration 2013, 2018). The fields are registered and stacked to create a deep master field, from which the list of stars is generated. Affine transforms are used to adjust the positions of the photometric apertures on each image, to compensate for any spacecraft pointing irregularities. After the photometry was extracted, a principal component analysis (PCA) of the brightest non-target stars was performed to remove systematic instrumental trends. The resulting normalized data are suitable for fitting with model transit light curves, and are discussed below.

3 ANALYSIS

With the normalized light curves in hand, the available parameter space was searched in order to find a transit model that best fit the system. In this effort, two publicly available pieces of software

* E-mail: cfox53@uwo.ca

Table 1. Priors for targets.

Parameter	WASP-43	TOI-1516	TOI-2046	Units
Planet radius	[0.0, 0.25]	[0.0, 0.2]	[0.0, 0.2]	R_s
LDC 1	[0.65, 0.75]	[0.25, 0.35]	[0.35, 0.45]	–
LDC 2	[0.0, 0.1]	[0.3, 0.4]	[0.2, 0.3]	–
Central time	[0.0, 1.0] + 2459695.5	[0.0, 1.0] + 2459391.8	[0.0, 1.0] + 2459423.5	BJD
Period	[0.6, 1.0]	[1.5, 2.5]	[1.0, 2.0]	d
Semimajor axis	[3.0, 6.0]	[2.0, 10.0]	[2.0, 7.0]	R_s
Inclination	[60.0, 90.0]	[60.0, 90.0]	[60.0, 90.0]	deg

were used. The transit modelling tool PYTRANSIT (Parviainen 2015) was used to create hypothetical model light curves based on a set of parameters. We adopted the quadratic model of Mandel & Agol (2002), the parameters of which are: planet radius, central transit time, period, semimajor axis, inclination, and two limb darkening coefficients. To find the light curve parameters that best fit the observations, the Bayesian analysis tool PYMULTINEST (Buchner et al. 2014) was used. Combined, these two pieces of software enabled us to search the parameter space that best fit the observed data, with our likelihood function based on the standard χ^2 metric.

To reduce the effects of longer term trends in the data that were not completely removed by the PCA, all observations used for generating the light curve and analysis were limited to within one transit duration of the expected central time (based on the Exoplanet Transit Prediction Service; Akeson et al. 2013). That is, if the transit had an expected duration of D , then we used observations from a time of $-D$ to $+D$ of the expected central transit time, with the expected transit occurring from $-D/2$ to $+D/2$.

In addition to computing system parameters, we also searched for Transit Timing Variations (TTVs) of each target. For each individual transit that showed a clear ingress or egress, we ran a separate Bayesian analysis. This used the best-fitting shape parameters from the entire light curve (derived from all transits), but fit the central transit time for each individual transit. The resultant best-fitting time for each individual transit was compared to the best-fitting times computed from the entire light curve (all transits). The difference provides an estimate of the timing variation of a particular transit event.

3.1 Priors

To fit the observed data to the parameters, our Bayesian fitting algorithm used seven priors: the planet radius, epoch time, orbital period, semimajor axis, inclination, and two limb darkening coefficients. Though the precise mechanism of hot Jupiter formation is still being debated, strong tidal dissipation resulting in orbital circularization is expected (Rasio & Ford 1996; Fabrycky & Tremaine 2007; Chernov, Ivanov & Papaloizou 2017). Thus our fits assumed eccentricity was zero for all runs.

The radius prior ran from 0 to +50 per cent of the initial value reported by *TESS*. The central transit time was arbitrarily chosen to be near the centre of one of the transits. The semimajor axis prior was set to be approximately ± 50 per cent of value of the value provided by the Exoplanet Transit Prediction Service (Akeson et al. 2013). Inclination values were allowed to range from 60 to 90 deg. The longitude of the ascending node is not needed by PYTRANSIT and was not fitted. The period prior was given a ± 0.25 d from the expected value. Because data were collected over multiple months and non-continuous, a tight period prior was required to prevent the fitting routine from settling into incorrect periods at integer multiples of the true period. All priors were uniform priors.

The model used for limb darkening was the quadratic model (Mandel & Agol 2002) as implemented by PYTRANSIT. The two Limb Darkening Coefficients (LDC) priors encompass ± 0.05 from the values provided for the star in question from the ExoPlanet Characterization Toolkit from the Space Telescope Science Institute (Stevenson et al. 2018). To create the LDC priors, we varied the effective temperature, surface gravity, and metallicity inputs of the Toolkit to the extent of their uncertainties. The resultant range of outputted LDC values (from one extreme to the other) were used as the range of the prior. Thus, these LDC priors account for uncertainties in the stellar effective temperature, surface gravity, and metallicity.

4 TARGETS

Of the three targets analysed here, two (TOI-1516.01 and TOI-2046.01) were classified as ‘planetary candidates’ by the NASA Exoplanet Archive at the time of observation; they were recently confirmed by Kabáth et al. (2022). Our third target was WASP-43b which is a previously ‘confirmed’ hot Jupiter.

4.1 WASP-43

Also known as TOI-656.01, WASP-43b is a well-studied ultrahot Jupiter (Hellier et al. 2011; Esposito et al. 2017; Patel & Espinoza 2022, among others). The host has an apparent visual magnitude $V = 12.3$ and is a K7 main sequence star (Hellier et al. 2011). The orbital period of the planet is 0.813 d. *NEOSSat* observations were taken on 2022 February 27, April 26, and May 24. The exposure time was 20 s with cadence also of 20 s. The priors used for this target are shown in Table 1.

Individual transit event data for WASP-43b are shown in Fig. 1, and the phase-folded light curve is shown in Fig. 2. The *NEOSSat* results for WASP-43b are largely consistent with other results (Hellier et al. 2011; Esposito et al. 2017), and are presented in Table 2. Our results suggest a slightly higher impact parameter than other sources (Esposito et al. 2017; Patel & Espinoza 2022). Because of the longer cadence and fewer observed transits, this target has the highest error among our three targets, but are within the mutual error bars of other sources. Of the three transits, one has excellent coverage of egress, and the other of ingress. Using these, we find all TTVs for observed events to be consistent with 0 ± 30 s.

4.2 TOI-1516

TOI-1516.01 is a planetary candidate observed by *TESS*, observed in FFI (full-frame-image) in Sectors 17 and 18. The host star is a $V = 10$ F8 main sequence star (Kabáth et al. 2022). *NEOSSat* observations were taken on 2021 March 28, May 14, May 18, June 26, September 2, and October 9. The exposure time was 5 s with a 10 s cadence.

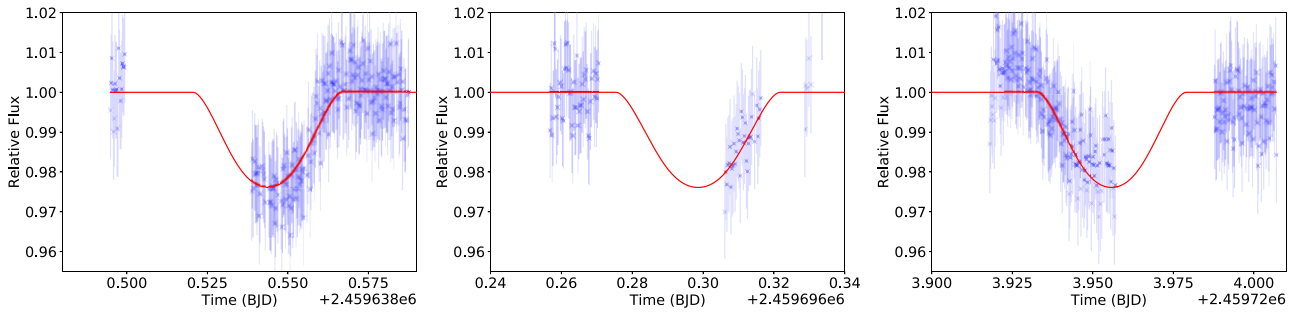


Figure 1. Normalized flux observations of WASP-43b. The red line is our fitted light curve.

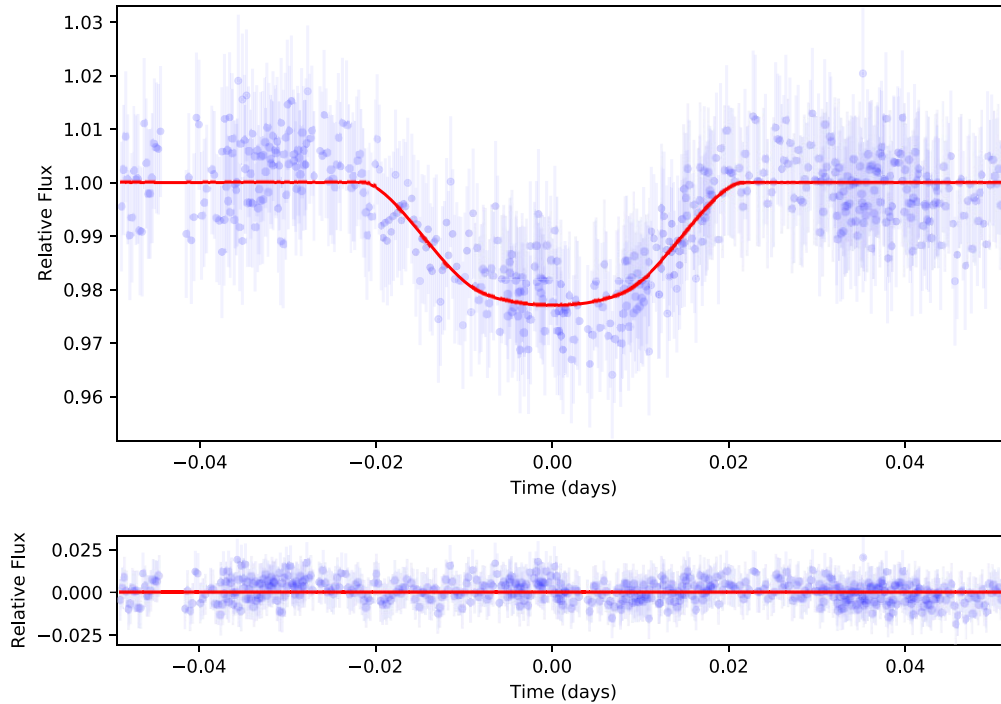


Figure 2. Phase-folded light curve and residuals of WASP-43b. The red line is the fitted light curve.

Table 2. Posteriors and computed properties for targets.

Parameter	WASP-43	TOI-1516	TOI-2046	Units
Planet radius	0.170 ± 0.018	0.1177 ± 0.0019	0.101 ± 0.002	R_s
LDC 1	0.699 ± 0.029	0.348 ± 0.029	0.391 ± 0.028	–
LDC 2	0.060 ± 0.029	0.250 ± 0.029	0.245 ± 0.029	–
Central time	$2459696.298550 \pm 0.000757$	$2459392.41028 \pm 0.00042$	$2459424.214180 \pm 0.000854$	BJD
Period	$0.81344697 \pm 0.00002370$	$2.05603408 \pm 0.00001256$	$1.49712564 \pm 0.00000816$	d
Semimajor axis	4.633 ± 0.251	5.834 ± 0.331	4.561 ± 0.252	R_s
Inclination	79.5 ± 1.1	87.02 ± 1.85	86.62 ± 2.35	deg
Impact parameter	0.837 ± 0.098	0.302 ± 0.187	0.272 ± 0.187	–
Total duration (t_{14})	1.117 ± 0.187	2.8738 ± 0.2375	2.672 ± 0.221	h
Stellar density	2.785 ± 0.465	0.901 ± 0.150	0.808 ± 0.136	g cm^{-3}

This planet was validated by Kabáth et al. (2022) after the *NEOSSat* observations were taken, but before the writing of this paper. The priors used for this target are shown in Table 1.

The individual transit events and folded curve are shown in Figs 3 and 4, respectively. Our results for TOI-1516.01, in Table 2, are consistent with what is already known of this hot Jupiter. The planet

has a radius 12 per cent of the host star’s. Four of the six transit events have good coverage of ingress, while a fifth has good egress coverage. Based upon these transits, we find no evidence of TTVs of more than 1 min. The *NEOSSat* results for TOI-1516.01 are consistent with initial values reported by *TESS* (from the Exoplanet Transit Prediction Service; Akeson et al. 2013) as well as Kabáth et al. (2022).

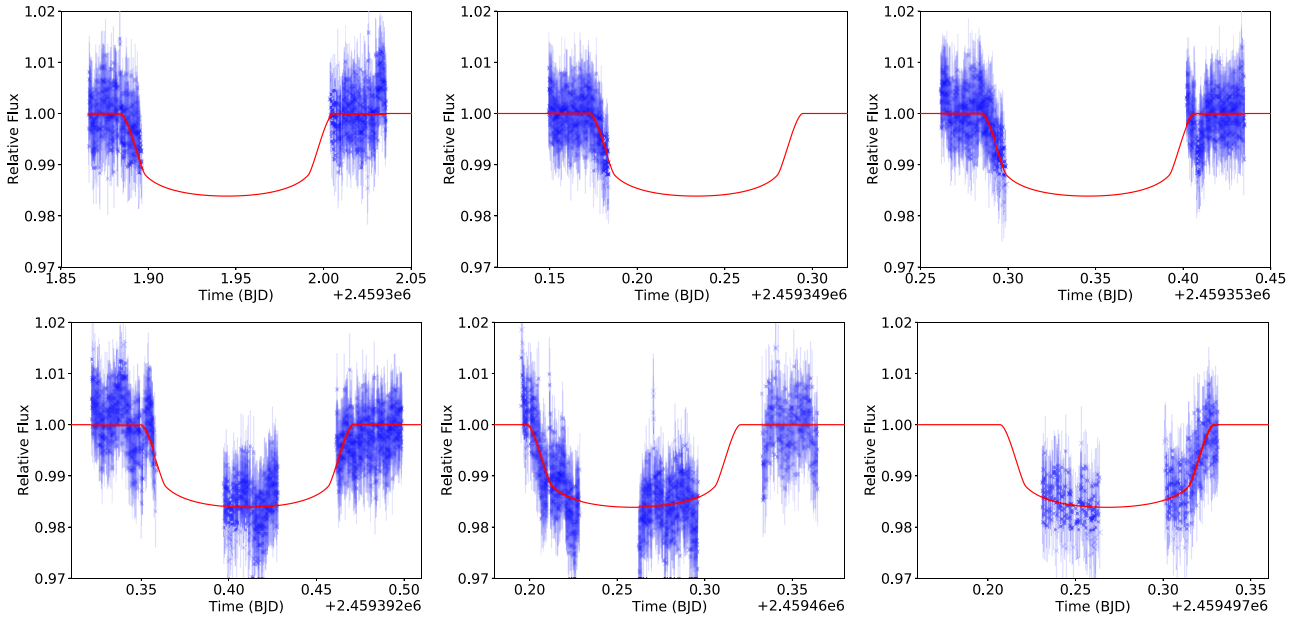


Figure 3. Normalized flux observations of TOI-1516.01. The red line is our fitted light curve.

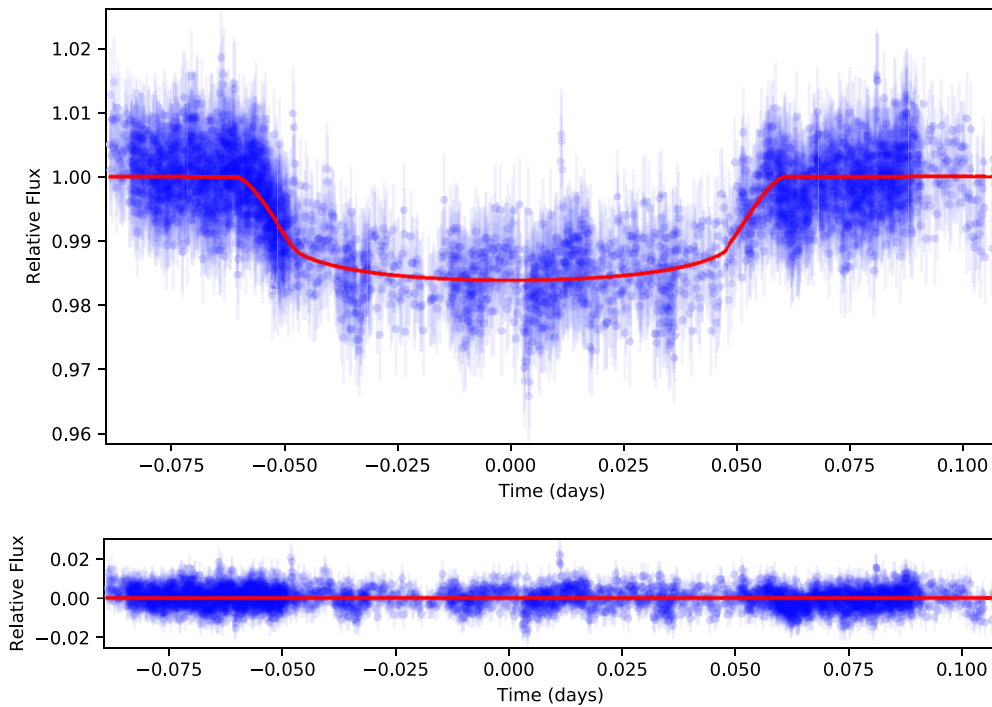


Figure 4. Phase-folded light curve and residuals of TOI-1516.01. The red line is our fitted light curve.

4.3 TOI-2046

TOI-2046.01 is a planetary candidate observed by *TESS*, observed in FFI (full-frame-image) in Sectors 18 and 19. The host star is a $V = 11.5$ F8 dwarf star (Kabáth et al. 2022). *NEOSSat* observations were taken on 2021 April 29, July 3, July 28, August 20, October 4, and November 22, and one observation on 2022 June 9. The exposure time was 7 s with a 10 s cadence. This planet was also validated by Kabáth et al. (2022) after the *NEOSSat* observations presented here were taken but before the writing of this paper. The priors used for this target are shown in Table 1.

The individual transit events are shown in Fig. 5, and the phase-folded light curve is shown in Fig. 6. Our results for TOI-2046.01, shown in Table 2, are consistent with the already-reported hot Jupiter nature of this system. Only two of our seven observed events have coverage of ingress, and only one covers egress. We see no indications of TTVs of larger than one minute. The *NEOSSat* results for TOI-2046.01 are consistent with initial values reported by *TESS* (from the Exoplanet Transit Prediction Service; Akesson et al. 2013) as well as Kabáth et al. (2022), with the exception of the planet:star radius. While Kabáth et al. (2022) reports a value of 0.1213 ± 0.0017 , we

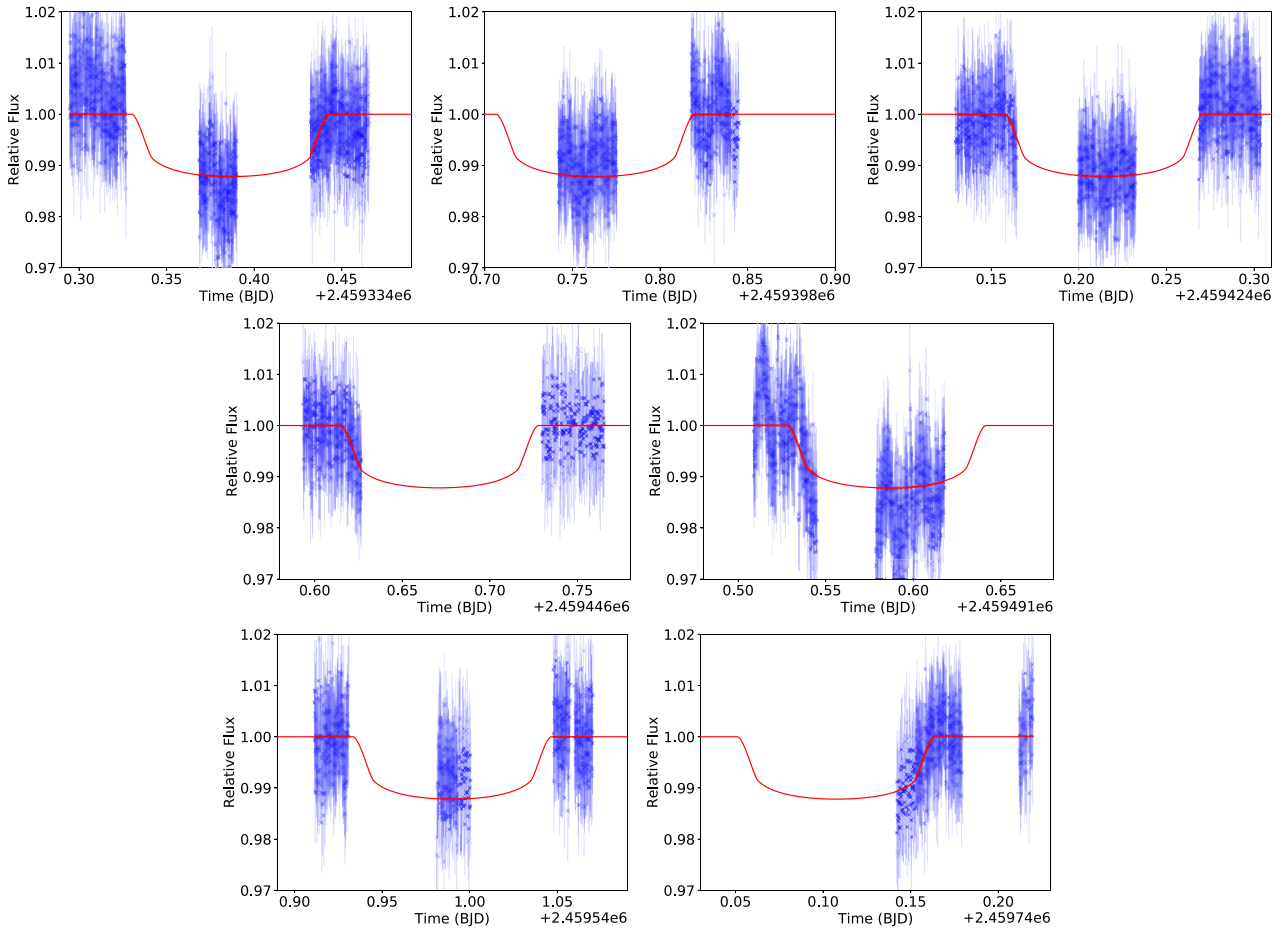


Figure 5. Normalized flux observations of TOI-2046.01. The red line is our fitted light curve.

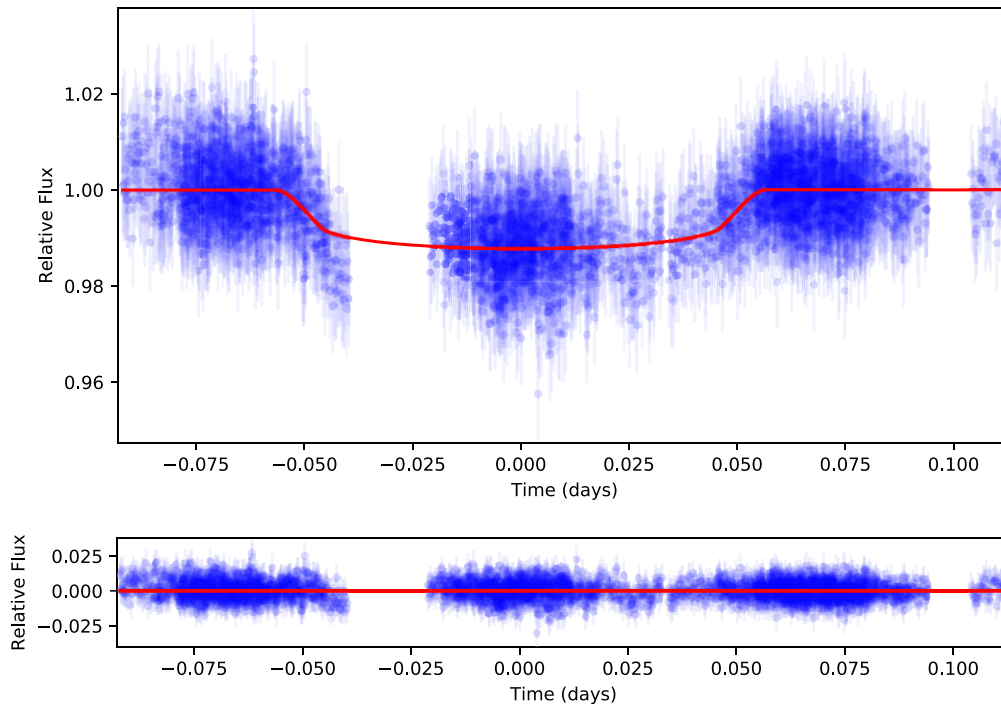


Figure 6. Phase-folded light curve and residuals of TOI-2046.01. The red line is our fitted light curve.

Table 3. Comparison of basic system parameters.

WASP-43 Parameter	This work	Hellier et al. (2011)	Esposito et al. (2017)	Patel & Espinoza (2022)	Units
Plan. Rad.	0.170 ± 0.018	–	0.1588 ± 0.0040	$0.1615^{+0.0017}_{-0.0025}$	R_s
Period	0.813447 ± 0.000024	0.813475 ± 0.000001	$0.813473978 \pm 0.000000035$	$0.8134749^{+0.0000009}_{-0.0000010}$	d
Semi. Axis	4.633 ± 0.251	–	4.97 ± 0.14	4.72 ± 0.05	R_s
Incl.	79.5 ± 1.1	$82.6^{+1.3}_{-0.9}$	82.109 ± 0.088	–	deg
Impact Par.	0.837 ± 0.098	–	0.689 ± 0.013	$0.698^{+0.012}_{-0.014}$	–
Dur. (t_{14})	1.117 ± 0.187	1.1592 ± 0.0264	1.16 ± 0.24	–	h
Stel. Dens.	2.785 ± 0.465	$2.939^{+0.971}_{-0.545}$	2.43 ± 0.14	–	g cm^{-3}
TOI-1516					
Parameter	This work	Kab�ath et al. (2022)	TESS Project (2022a)		Units
Plan. Rad.	0.1177 ± 0.0019	$0.1224^{+0.0005}_{-0.0005}$	0.1212 ± 0.0052	–	R_s
Period	2.056034 ± 0.000012	$2.056014^{+0.000002}_{-0.000002}$	2.05603 ± 0.00001	–	d
Semi. Axis	5.834 ± 0.331	$6.22^{+0.041}_{-0.077}$	–	–	R_s
Incl.	87.02 ± 1.85	90.0 ± 0.4	–	–	deg
Impact Par.	0.302 ± 0.187	$0.09^{+0.10}_{-0.07}$	–	–	–
Dur. (t_{14})	2.8738 ± 0.2375	$2.826^{+0.015}_{-0.014}$	2.829 ± 0.015	–	h
Stel. Dens.	0.901 ± 0.150	1.090 ± 0.031	0.97417 ± 0.219076	–	g cm^{-3}
TOI-2046					
Parameter	This work	Kab�ath et al. (2022)	TESS Project (2022b)		Units
Plan. Rad.	0.101 ± 0.002	$0.1213^{+0.0017}_{-0.0021}$	0.1354 ± 0.0116	–	R_s
Period	1.49712564 ± 0.0000082	$1.4971842^{+0.0000031}_{-0.0000033}$	1.497	–	d
Semi. Axis	4.561 ± 0.252	$4.75^{+0.18}_{-0.17}$	–	–	R_s
Incl.	86.62 ± 2.35	83.6 ± 0.9	–	–	deg
Impact Par.	0.272 ± 0.187	$0.51^{+0.06}_{-0.07}$	–	–	–
Dur. (t_{14})	2.672 ± 0.221	$2.410^{+0.032}_{-0.030}$	2.806 ± 0.178	–	h
Stel. Dens.	0.808 ± 0.136	0.890 ± 0.098	0.835862 ± 0.183146	–	g cm^{-3}

find a value of 0.101 ± 0.002 . This difference is likely caused by some remaining systematic trends in the *NEOSSat* photometry.

5 RESULTS AND ANALYSIS

5.1 Comparison to other results

The purpose of this observing campaign was to demonstrate *NEOSSat* as a useful follow-up contributor to exoplanet science. However, for the particular systems targeted here, many of our results have been anticipated by the study of Kab ath et al. (2022) which examined two of our three targets, and which was published during the preparation of this work. As a result, though some of our results duplicate theirs, a comparison provides some insight into *NEOSSat*'s performance vis-a-vis other techniques and systems currently in use.

5.2 Basic system parameters

In Table 3 we summarize the results of this paper together with established values from other sources. Our results are largely consistent with other studies; our returned values are within the mutual error bars of the other sources. Thus *NEOSSat* is capable enough to provide basic exoplanetary system parameters with an accuracy comparable to that of other current observing platforms.

5.3 Transit ephemeris

The ephemeris we find for these targets is consistent with those of *TESS*. Using the central transit times from the *TESS* Project Candidate data (TESS Project 2022a,b,c) (depending on the target) as an initial start date, and the *TESS* computed period, we can estimate the difference between our computed central transit times and those

expected from the *TESS* ephemeris. For WASP-43b, TOI-1516.01, and TOI-2046.01 our central transit times are within 6.0, 3.7, and 0.9 min, respectively (see Table 4). Thus *NEOSSat* can produce central transit times consistent with other observatories.

Using the *TESS* results also gave us a longer baseline which enabled us to compute a new higher precision ephemeris. For TOI-1516.01, the resultant error on the period was reduced from 10^{-5} to 1.5×10^{-6} d. In the case of TOI-2046.01, the error was reduced from 10^{-4} (no error estimate is provided by the *TESS* Project, so we presumed the last digit) to 2.2×10^{-6} d. Our refined ephemeris for WASP-43b has a much higher error than the *TESS* project's, likely due to the very low error provided by the *TESS* Project. This very low error is likely due to extending the baseline back to the initial WASP observations in 2010. However, when combining our data with the *TESS* results, our refined ephemeris is within 4×10^{-6} d (approximately 0.5 s) of other sources (Esposito et al. 2017; Patel & Espinoza 2022, among others). The updated ephemeris results are shown in Table 4. Thus *NEOSSat* can be useful in refining orbital periods.

6 SUMMARY

In this study, we examined three hot Jupiters to demonstrate the capabilities of *NEOSSat* as a tool for exoplanet science. We have demonstrated that *NEOSSat* can return exoplanetary parameters consistent with other dedicated exoplanet missions (such as *TESS*), even with incomplete transits events. Further, we used the results to improve the orbital ephemeris of these targets. *NEOSSat* can be a useful tool for confirming and/or improving parameters.

However, there are some complications. Because *NEOSSat* is generally limited to continuous viewing times of an hour, and transit durations are usually longer than this, finding brand new planets is a more difficult task. A brand new planet could potentially have a

Table 4. Refined ephemeris for targets.

	WASP-43b	TOI-1516.01	TOI-2046.01	
<i>TESS</i> T_c	2459279.797452 ± 0.000067	2458765.32531 ± 0.00019	2458792.39519 ± 0.00038	BJD
<i>TESS</i> period	0.813473629 ± 0.00000029	2.05603 ± 0.00001	1.4972	d
<i>TESS</i> expected T_c	2459696.295950 ± 0.000149	2459392.41446 ± 0.00305	2459424.21359 ± 0.00038	BJD
Our T_c	2459696.298550 ± 0.000757	2459392.410283 ± 0.000423	2459424.214180 ± 0.000854	BJD
<i>TESS</i> expected T_c - Our T_c	-0.002560 ± 0.000772	0.004177 ± 0.003079	-0.000590 ± 0.000935	d
Baseline length	416.5011 ± 0.000760	627.084973 ± 0.000464	631.81899 ± 0.000935	d
Number of orbits	512	305	422	
Resultant period	0.81347871 ± 0.00000148	2.05601631 ± 0.00000152	1.497201398 ± 0.00000222	d

period only known to an integer multiple due to the non-continuous nature of the coverage. If certain stellar parameters can be known independently, then this period degeneracy could be reduced. In such a case, multiple observations could be combined to produce a single curve with well-established parameters useful for followup science.

ACKNOWLEDGEMENTS

We thank the anonymous reviewer for their feedback that helped us improve this work. We also thank the *NEOSSat* Team at the Canadian Space Agency for their dedicated and enthusiastic help. This research has made use of the NASA Exoplanet Archive, which is operated by the California Institute of Technology, under contract with the National Aeronautics and Space Administration under the Exoplanet Exploration Program. This research used the facilities of the Canadian Astronomy Data Centre operated by the National Research Council of Canada with the support of the Canadian Space Agency. This work was funded in part by the Natural Sciences and Engineering Research Council of Canada Discovery Grants program (Grant no. RGPIN-2018-05659).

DATA AVAILABILITY

All data used in this paper comes from publicly available sources including NASA's Exoplanet Archive at <https://exoplanetarchive.ipac.caltech.edu> (Akeson et al. 2013). Raw *NEOSSat* data are available online from the Canadian Astronomy Data Centre at <https://www.cadccda.hia-ihc-nrc-cnrc.gc.ca/en/> (Crabtree et al. 1994).

REFERENCES

Akeson R. L. et al., 2013, *PASP*, 125, 989
 Astropy Collaboration 2013, *A&A*, 558, A33

Astropy Collaboration 2018, *AJ*, 156, 123
 Buchner J. et al., 2014, *A&A*, 564, A125
 Chernov S. V., Ivanov P. B., Papaloizou J. C. B., 2017, *MNRAS*, 470, 2054
 Crabtree Dennis and Durand, D. and Fisher, W. and Gaudet, Séverin and Hill, N. and Justice, G. and Morris, S. and Woodsworth, A., 1994, *Astronomical Data Analysis Software and Systems III ASP Conference Series*, 61, 123
 Esposito M. et al., 2017, *A&A*, 601, A53
 Fabrycky D., Tremaine S., 2007, *ApJ*, 669, 1298
 Hellier C. et al., 2011, *A&A*, 535, L7
 Kabáth P. et al., 2022, *MNRAS*, 513, 5955
 Laurin D., Hildebrand A., Cardinal R., Harvey W., Tafazoli S., 2008, in Oschmann J. M., Jr., de Graauw M. W. M., MacEwen H. A., eds, *Proc. SPIE Conf. Ser. Vol. 7010, Space Telescopes and Instrumentation 2008: Optical, Infrared, and Millimeter*. SPIE, Bellingham, p. 34
 Mandel K., Agol E., 2002, *ApJ*, 580, L171
 Parviainen H., 2015, *MNRAS*, 450, 3233
 Patel J. A., Espinoza N., 2022, *AJ*, 163, 228
 Rasio F. A., Ford E. B., 1996, *Science*, 274, 954
 Ricker G. R. et al., 2014, in Oschmann Jacobus M. J., Clampin M., Fazio G. G., MacEwen H. A., eds, *Proc. SPIE Conf. Ser. Vol. 9143, Space Telescopes and Instrumentation 2014: Optical, Infrared, and Millimeter Wave*. SPIE, Bellingham, p. 914320
 Rowe J., 2020, Source Code for the CSA's *NEOSSat* Mission. Available at: <https://github.com/jasonfrowe/neossat>
 Stevenson K. et al., 2018, *American Astronomical Society Meeting Abstracts* #231, 148.14
 TESS Project, 2022a, TOI-1516 ExoFOP page. Available at: exofop.ipac.caltech.edu
 TESS Project, 2022b, TOI-2046 ExoFOP page. Available at: exofop.ipac.caltech.edu
 TESS Project, 2022c, TOI-656 ExoFOP page. Available at: exofop.ipac.caltech.edu

This paper has been typeset from a $\text{\TeX}/\text{\LaTeX}$ file prepared by the author.